Open Access

Optimization of PC micro-drilling using a continuous CO_2 laser: an experimental and theoretical comparative study

Ansam E. Abdulwahab[1], Kadhim A. Hubeatir[1*] and Khalil I. Imhan[2]

*Correspondence:
Kadhim.A.Hubeatir@uotechnology.
edu.iq

[1] Department of Laser and
Optoelectronics Engineering,
University of Technology, Baghdad,
Iraq
Full list of author information is
available at the end of the article

Abstract

Laser drilling on polymers has many applications in various industries, such as sensors, aerospace, medical devices, and microelectronics. In this research, a CO_2 laser machine was employed for micro-drilling PC samples. Design–Expert analysis was applied to understand the laser drilling process better. Based on a Box–Behnken design (BBD) of the experimental software, 17 experiments were designed to examine the laser parameters' influence on the micro-drilling process. The impact of parameters, such as power (P), exposure time (t), and focal plane position (FPP), on the depth, entry diameter, and heat-affected zone (HAZ) was investigated using analysis of variance (ANOVA). Quadratic regression models were applied to model different hole factors throughout the process. The experiments were optimized using the developed objective model as a function to attain the best hole. The outcomes revealed that a full hole with a 351-μm diameter and 102-μm HAZ was obtained at 0 FPP, with a laser power of 4 W, and at 0.15 s. To conduct virtual tests alongside the experimental study, simulation of the drilling mechanism's temperature distribution was achieved via the COMSOL Multiphysics program. The simulation's refined accuracy was able to predict the hole's geometry and presented outcomes that favorably corresponded with the experimental results. A numerical optimization technique was used to generate an ideal hole by minimizing or maximizing the objective function, achieving full holes of 350-μm diameter and 90-μm HAZ, obtained at 0 FPP, with 3.6 W, and at 0.1 s.

Keywords: Laser drilling, CO_2 laser, Polycarbonate, COMSOL, ANOVA, BBD

Introduction

Drilling is one of the oldest machining processes for creating various holes. With the development of materials and the demand for holes with high precision at a greater drilling rate, laser drilling is more practical than other traditional machining processes. It has a higher productivity rate for a wide variety of materials such as metals, wood, and polymers. It is also lower in cost compared to the CNC laser cutter [1–7]. Laser micromachining is also employed in biomedical activities, e.g., tissue engineering and biochips [8, 9].

The drilling procedure of the laser drilling technique is accomplished by converting optical power to thermal power. When the temperature of the element reaches a

Abdulwahab *et al. Journal of Engineering and Applied Science*   (2022) 69:98

Page 2 of 16

melting and/or vaporization point, the hole begins to form throughout different processes depending on the temperature of said element. Melting occurs without vaporization when the temperature falls below a certain threshold (typically around 500°C for PC). To complete the drilling operation, the melted object is ejected through the use of an assist gas jet. If laser radiation exceeds a certain threshold, its drilling debris is accomplished by evaporation [10–14].

Laser drilling involves several parameters, such as power, focal plane, exposure time (for CW laser) or pulse duration (for pulsed lasers), frequency, and wavelength. All parameters must be controlled to attain ideal hole features. The hole's quality is essential for field applications [15]. Circularity, taper angle, barreling, and debris formation are all elements of a good product hole. The taper angle is, by definition, the angle formed by the drilled holes whose exit diameter is less than the entrance diameter. Hole circularity is measured by the difference in the diameter's upper and lower limits just at the hole entry [16]. Feret's diameter can also be used to describe circularity at the entry surface area of the workpiece hole [17]. The barreling determines the similarity of the hole's sides. The recast layer placed on the workpiece surface from around the tunnel is referred to as spatter. Chen and Hu investigated the effects of power on the width of fabricated microchannels on a polycarbonate substrate. They discovered that as the power increases, the diameter of the hole expands [18].

Various laser types have been used throughout multiple industries for drilling, such as fiber laser, CO_2 laser, semiconductor laser, excimer laser, and Nd: YAG laser [19]. CO_2 is still the most productive and cost-effective drilling laser for polymers. Polymers are not electricity or heat conductors. The organic matter absorbs significant beam energy at 10.6-µm wavelength [20–25].

Polycarbonate has gained tremendous attention in the last decade due to its widespread application, replacing wood and steel. It possesses thermal properties that make it an effective heat insulator in sensors, and it is relatively inexpensive [23]. This material is suitable for laser micro-drilling since it has an 89% absorption rate for carbon dioxide radiant energy, lower thermal capacity, poor thermal conductivity, and lower temperature decay [18]. The surface can also be adapted for the fabrication of microelectronic thin-film circuit boards.

The purpose of this research is to practically and theoretically analyze the influence of continuous CO_2 laser parameters on polycarbonate material by using the Design–Expert program. COMSOL Multiphysics software is also applied to simulate the temperature distribution of the PC sample during laser drilling. Due to the polycarbonate's properties, the laser drilling process produces an opaque yellow color on the plane as well as burnt edges. Appropriate selection of laser drilling process parameters improves hole quality and eliminates burnt edges in this operation. This has not been observed in previous studies. The outcomes can optimize various microelectronic and microfluidic applications.

Methods

In this research, laser drilling was conducted on a polycarbonate (7 cm × 3 cm × 1 mm) using a CNC continuous CO_2 laser with a 10.6-µm wavelength from the JK series. The Laser Cut 53 computer-aided design (CAD) program was applied to
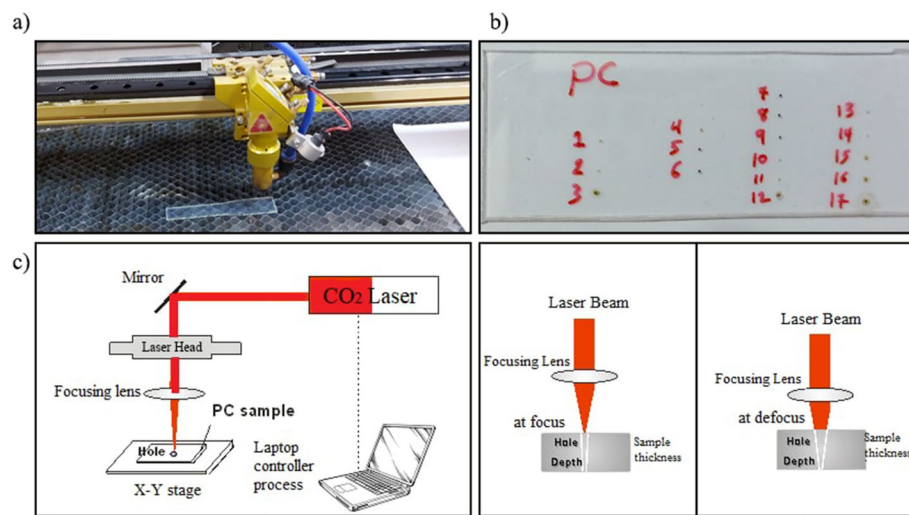
Fig. 1 a The experimental setup of laser drilling. **b** PC sample. **c** Schematic diagram of the CO_2 laser micromachining system

Table 1 Input parameter variation ranges in DOE

Parameters	Sign	Unit	−1	0	1
A-Power	P	W	2	3	4
B-Exposure time	t	s	0.1	0.15	0.2
C-FPP	FPP	mm	−4	−2	0

control the machine using manually defined instructions. The laser was directed at the polycarbonate plate using a lens with a focal length of 58 mm (see Fig. 1). The laser spot size on the sample was 300 μm. The material absorbs the laser beam's energy, causing a surface temperature increase.

Box–Behnken design (BBD)

Box–Behnken design (BBD) was chosen to investigate the influence of three input continuous CO_2 laser drilling process variables—laser power, exposure time, and focal plane position (FPP)—on the hole geometry of a polycarbonate sheet of 1-mm thickness. Different process parameters were chosen in an experimental setting based on the ability of the laser source to change these parameters. A survey of laser drilling and cutting publications was accomplished before conducting the experiments. Table 1 displays the variation levels (−1, 0, 1) of the input parameters. The FPP was considered to be 0 when placed on the workpiece surface's upper area. The lower and upper FPP surfaces were classified as negative and positive, respectively, as shown in Fig. 1. The properties of the materials are tabulated in Table 2. Tests were performed on the polycarbonate based on Design−Expert software, according to the experimental plan depicted in Table 3. Then, the entry diameter, depth, and HAZ were measured using a microscope at 50 × magnification for each run (each

Abdulwahab *et al. Journal of Engineering and Applied Science*   (2022) 69:98

Page 4 of 16

Table 2 Polycarbonate properties used in the simulation [26–31]

Density (g/cm³)	Specific heat (kJ/kg)	Thermal conductivity (W/m K)	Vaporization temperature (°C)	Melting temperature (°C)	Thermal expansion coefficient (10–6 1/K)	Absorptivity % of CO_2
1.2	1.3	0.22	500	240	70	89

Table 3 Experimental results of the effect of laser power, exposure time, and FPP on the diameter, depth, and HAZ of drilled holes, as presented by Design–Expert software

No.	Factor 1	Factor 2	Factor 3	Response 1	Response 2	Response3
Run	A: Power (W)	B: Exposure time (s)	B: FPP (mm)	Depth of hole (mm)	Diameter of hole (µm)	HAZ (µm)
1	2	0.15	−4	0.4	500	155
2	2	0.2	−2	0.7	350	102
3	2	0.1	−2	0.4	320	80
4	2	0.15	0	0.8	320	80
5	3	0.1	−4	0.4	565	118
6	3	0.2	−4	0.82	618	206
7	3	0.15	−2	0.65	340	100
8	3	0.15	−2	0.651	341	100.2
9	3	0.15	−2	0.65	341	100
10	3	0.15	−2	0.65	340.7	100.05
11	3	0.15	−2	0.6502	340	100
12	3	0.1	0	0.8	331	80
13	3	0.2	0	1	400	101
14	4	0.15	−4	0.8	616	170
15	4	0.1	−2	1	352	101
16	4	0.2	−2	1	500	202
17	4	0.15	0	1	351	102

run required nine readings in addition to more than three repetitions of the middle value). Table 3 provides the mean values of the entry diameter, depth, and HAZ depending on BBD.

ANOVA was used to analyze the responses (output parameters) influenced by a number of factors (input parameters). Changes in the input variables were made in each experiment to determine the reason behind different response variables. The goal was to construct a mathematical model that represented a link between inputs and outputs (parameters and responses) with the fewest mistakes. Variable parameters differed depending on the input type.

A general quadratic equation was applied to predict the response for different levels of each factor, as given by [32]:

$$y = \beta_o + \sum\nolimits_{i=1}^{m} \beta_i x_i + \sum\nolimits_{i=1}^{m} \beta_{ii} x_i{}^2 + \sum\nolimits_i \sum\nolimits_j \beta_{ij} x_i x_j + \varepsilon \tag{1}$$

where m is the number of parameters, β is the constant, β_i is the linear coefficient, β_{ii} is the quadratic coefficient, β_{ij} is the interaction coefficient, and ɛ is the parameter's error.

COMSOL Multiphysics 5.6 software

COMSOL software was employed for the simulation of CO_2 laser interactions with the polycarbonate plate using the previously mentioned experimental parameters. 3D transparent polycarbonate material was created within the program, as shown in Fig. 2a. The series of holes was executed through the drilling simulation. The final shape is depicted in Fig. 2b. The CO_2 laser was aimed at the sample's top surface, and the holes were drilled perpendicular to the surface. Some laser characteristics (e.g., power, FPP, and exposure time) were modified in a systematic manner, whereas others remained constant, as presented in Table 1.

The technique for measuring each parameter's effect was to change only one variable in each test while keeping the remaining values constant. This approach provides a better understanding of the holes' evolution in each CO_2 beam parameter increase throughout the modeling of the drilling process.

The surface materials were chosen from the COMSOL library. As a result, the elemental composition of PC is defined in the simulation program. Table 2 displays the most essential properties of the material for the modeling depending on the temperature in this work.

The distribution of the laser power varies within the laser beam's spot. The highest is at the center and then diminishes towards the periphery [33]. For the zero focus position, the laser radiation was aimed at the top surface. The diameter of the CO_2 laser was calculated from the following equation [34]:

$$d_f = \frac{1}{\pi} \left(\frac{f_1 \lambda}{d_0} \right) \tag{2}$$

where f_1 represents the focal length of the focusing lens in mm, λ is the laser's wavelength used, and d_0 represents the laser beam's diameter before adjusting the lens' focus.

As for the defocused position laser drilling, the laser beam was set to strike a surface at the defocus distances of −2 and −4 mm. The defocus distances were chosen to keep the diameter of the beam spot below 500 μm at the hit surface. The larger spot size may result in a bigger hole diameter, more than the 500-μm range. The laser beam radius at the defocus distance can be calculated using Eq. 4 [35]:
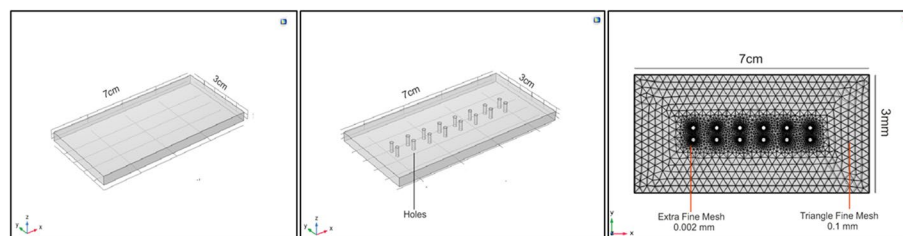

Fig. 2 **a** 3D PC structure before irradiation, **b** laser beam drilling of several holes on a 3D PC sample, and **c** 2-dimensional mesh of a sample refined along with all laser spot sizes

Abdulwahab *et al. Journal of Engineering and Applied Science*   (2022) 69:98

Page 6 of 16

$$w = w_i \left[1 + \left(M^2 \frac{\lambda(z)}{\pi w_i{}^2} \right)^2 \right]^{\frac{1}{2}} \tag{3}$$

where z is the depth from the focal plane; w is the beam radius at z; w_i represents the original laser beam radius at the focus plane; M^2 is the beam quality factor, which is equal to 1.5 (according to the laser manufacturer's registration); and λ represents the laser beam's wavelength.

Free triangle mesh was applied for all workpieces with size 0.1 mm. Such meshing does not require a long time to process. However, *extra fine mesh* was used for the beam spot size of size 0.002mm, which is regarded as the minimum element size, as shown in Fig. 2c. Fine meshing can result in more sophisticated peak temperature predictions.

This thermal model is proposed to compute the depth, HAZ, and diameter of the resulting sample after CO_2 radiation. By applying heat transfer to the sample's surface, materials with a temperature greater than their melting point are removed from the sample surface.

The simulation's objective is to evaluate the parameters that will enable us to achieve an optimized hole diameter with the lowest cost. Simulations are also the best approach for predicting this process' thermomechanical behavior.

Results and discussion

The results and discussion are divided into several parts, as follows.

Statistical analysis

The hole depth

Table 4 presents a variance analysis for the depth model. This table is the result of removing inefficient factors. The *p*-value illustrates how each factor affects the depth. The probability value is calculated under the assumption of "0". If the *p*-value for each parameter is less than 0.05, this indicates that the parameter influences the depth, further proving the model's relevance. The R^2 values represent the quantity of data covered by the regression model. The quadratic regression equation for the depth is provided in Eq. 4. The final regression equation acquired also proved to be a good model for predicting and

Table 4 Variance analysis of the depth

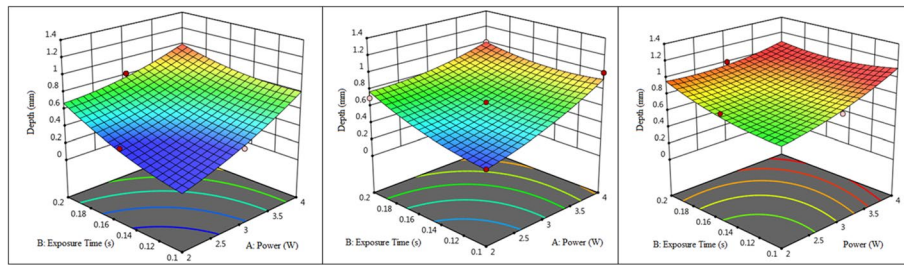| Source	Sum of squares	df	Mean square	*F*-value	*p*-value	R^2
Model	0.6496	9	0.0722	20.96	0.0003	0.9642
A-power	0.2813	1	0.2813	81.69	< 0.0001	Significant
B-exposure time	0.1058	1	0.1058	30.73	0.0009	
C-FPP	0.1741	1	0.1741	50.55	0.0002	
AB	0.0225	1	0.0225	6.54	0.0378	
AC	0.0100	1	0.0100	2.90	0.1321	
BC	0.0121	1	0.0121	3.51	0.1030	
A^2	0.0151	1	0.0151	4.38	0.0745	
B^2	0.0177	1	0.0177	5.15	0.0576	
C^2	0.0067	1	0.0067	1.94	0.2058	

Fig. 3 The hole depth curve for exposure time and power at FPP: **a** −4 mm, **b** −2 mm, and **c** 0 mm
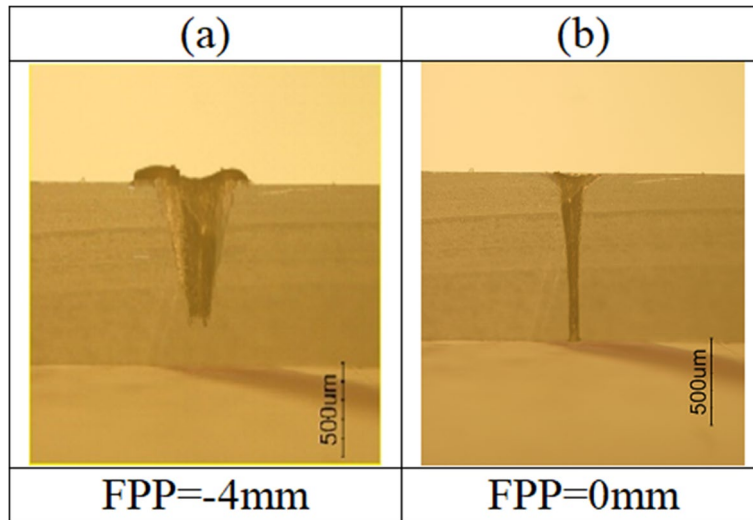

Fig. 4 The shape of depth variation when irradiated with a laser exposure time of 0.15s and power of 4 W at different FPPs: **a** −4 and **b** 0, respectively

evaluating the impact of parameters. Figure 3 displays a three-dimensional graph with the highest depth obtained at −2 mm, zero distance from the sample surface, and with a power of 4 W. When the power was reduced to 3 W, the depth reduced at −2 FPP, while the entire hole remained at 0 FPP from the PC sheet surface. Due to the obvious Gaussian laser beam energy distribution, the energy input varied at different areas within the beam diameter. The highest energy density was at the center of the beam, while the lowest was at the outer end. Figure 4 displays the microscopic images of the depth with different FPPs at 0.15s and 4 W. With focus processing, the depth had a V-shaped cross-section. However, during the defocus process, it took on a U-shape.

$$\mathrm{Depth} = +0.6 + 0.003 * \mathrm{P} - 2.08 * \mathrm{t} + 0.2\,\mathrm{FPP} - 1.5 * \mathrm{P} * \mathrm{t} - 0.025 * \mathrm{P} * \mathrm{FPP}$$
$$- 0.55 * \mathrm{t} * \mathrm{FPP} + 0.05 * \mathrm{P}^2 + 25.9 * \mathrm{t}^2 + 0.009 * \mathrm{FPP}^2 \tag{4}$$

The entry hole diameter

The FPP parameter has the highest influence on the hole diameter, according to Table 5. Equation 5 further depicts a regression relationship for the diameter. Figures 5 and 6 show

Abdulwahab *et al. Journal of Engineering and Applied Science*   (2022) 69:98

Page 8 of 16

Table 5 Analysis of the diameter

Source	Sum of squares	df	Mean square	*F*-value	*p*-value	R^2
Model	1.824E+05	9	20263.09	256.83	< 0.0001	0.9970
A-power	13530.13	1	13530.13	171.49	< 0.0001	
B-exposure time	11250.00	1	11250.00	142.59	< 0.0001	
C-FPP	1.006E+05	1	1.006E+05	1274.77	< 0.0001	
AB	3481.00	1	3481.00	44.12	0.0003	
AC	1806.25	1	1806.25	22.89	0.0020	
BC	64.00	1	64.00	0.8112	0.3977	
A^2	70.95	1	70.95	0.8993	0.3746	
B^2	5412.97	1	5412.97	68.61	< 0.0001	
C^2	43896.55	1	43896.55	556.37	< 0.0001	
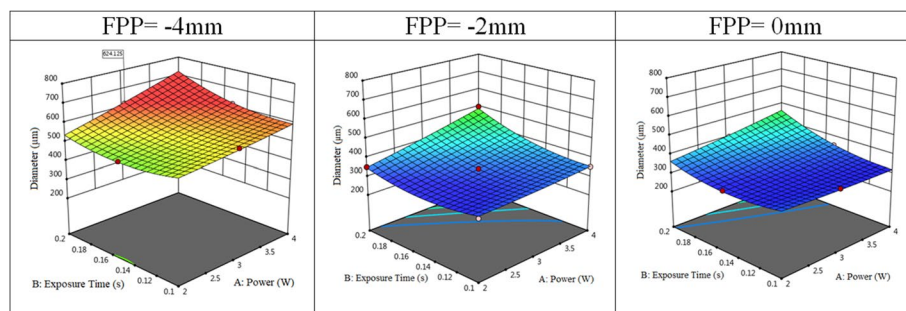
Fig. 5 The effect of laser power, exposure time, and FPP on the entry diameter
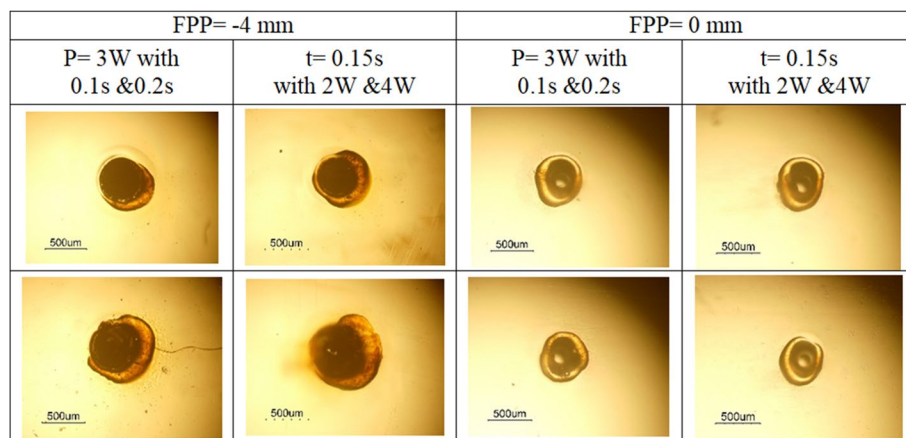
Fig. 6 The shape and diameter variation of the holes at the top surface when irradiated with laser powers of 2, 3, and 4 W at different exposure times (0.1, 0.15, and 0.2s) and different FPPs (−4 and 0mm)

how laser power and exposure time have a direct relationship with the diameter. Increasing the contact time with the material leads to enlargements and deformations of the hole since the material was exposed to greater heat for a longer period of time. The hole diameter at focus remains lower than the hole diameter at defocus due to the decrease in laser beam spot diameter. The greatest result for the entry diameter was 618 μm at a focal plane distance of −4 from the sample surface. This is consistent with the findings of a recently published study [36].

Table 6 The analysis of HAZ

Source	Sum of squares	df	Mean square	F-value	p-value	R²
Model	24995.01	9	2777.22	21.45	0.0003	0.9650
A-power	3120.50	1	3120.50	24.10	0.0017	
B-exposure time	6728.00	1	6728.00	51.95	0.0002	
C-FPP	10224.50	1	10224.50	78.95	< 0.0001	
AB	1560.25	1	1560.25	12.05	0.0104	
AC	12.25	1	12.25	0.0946	0.7674	
BC	1122.25	1	1122.25	8.67	0.0216	
A²	495.67	1	495.67	3.83	0.0913	
B²	451.04	1	451.04	3.48	0.1043	
C²	1057.78	1	1057.78	8.17	0.0244	
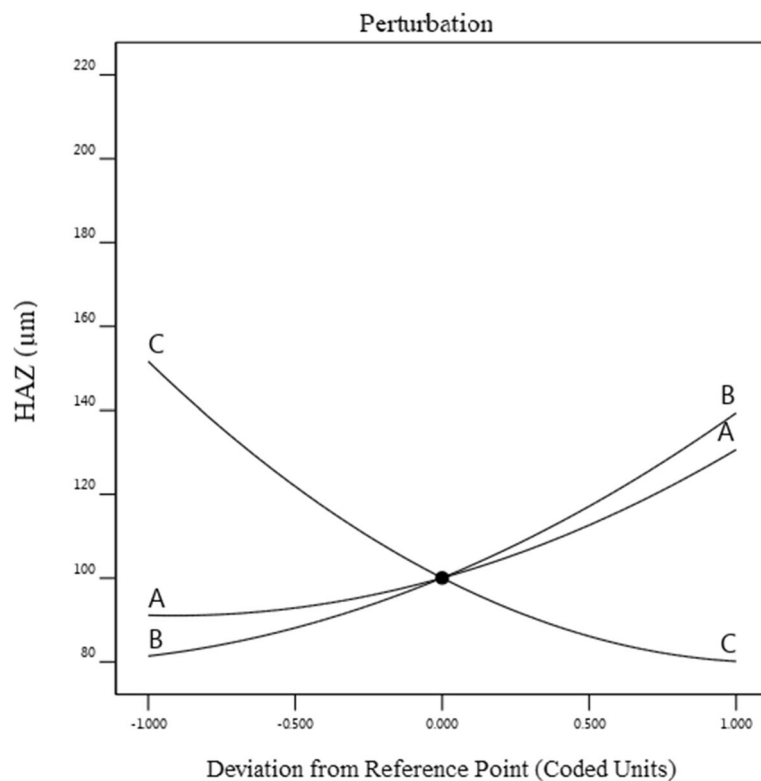
Fig. 7 The impact of various factors on HAZ

$$Diameter = +771.5 - 93.2 * P - 5242.6 * t + 71.9 * FPP + 590 * P * t - 10.6 * P * FPP$$
$$- 10.6 * P * FPP + 40 * t * FPP + 4.1 * P^2 + 14342 * t^2 + 25.5 * FPP^2 \tag{5}$$

The heat-affected zone of the hole

Various input factors have a similar influence on the HAZ, as shown in Table 6. Equation 6 describes the regression equation for HAZ. Figure 7 demonstrates the impact of
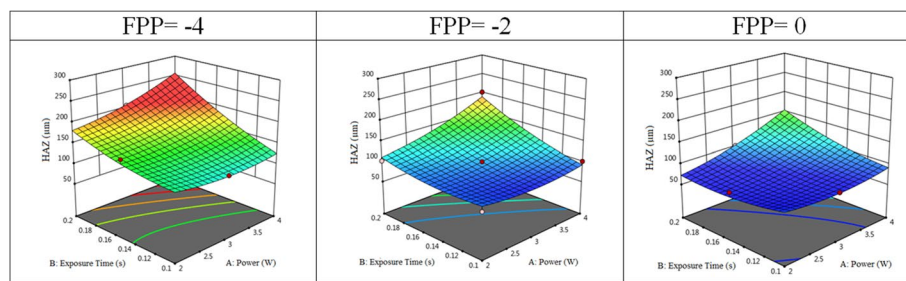
Fig. 8 The 3D surface of HAZ with different factors

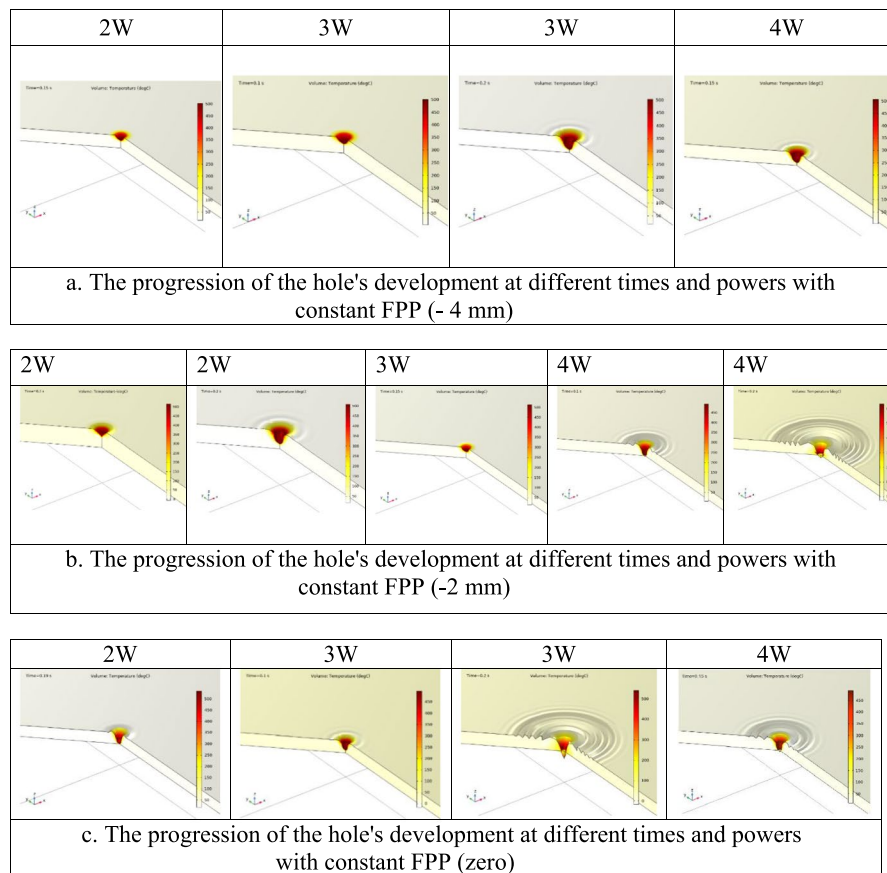**Fig. 9 a** The progression of the hole's development at different times and powers with constant FPP (−4 mm). **b** The progression of the hole's development at different times and powers with constant FPP (−2 mm). **c** The progression of the hole's development at different times and powers with constant FPP (0)

various input parameters on HAZ. The results indicate that the laser power and time play a significant role on HAZ. As the power and time increase, the region of HAZ significantly increases due to receiving higher energy by the sample. Figure 8 shows how the size of HAZ expands as the laser FPP penetrates deeper through the material. The largest beam energy amount is towards the bottom of the piece at defocus, resulting in

a greater heat-affected zone. Figure 9 presents the lowest HAZ which occurred at 0 FPP with 0.15s and 2 W, while the highest HAZ occurred at −4mm FPP.

$$
\begin{aligned}
HAZ = {}& +347.45 - 102.85 * P - 2182 * t + 20.475 * FPP + 395P * t + 0.875 * P * FPP \\
& - 167 * t * FPP + 10.85\,P^2 + 4140 * t^2 + 3.9 * FPP^2
\end{aligned}
\tag{6}
$$

Thermal analysis

Simulations of experiments were conducted depending on the Box–Behnken design (BBD). The CO_2 laser heating of the material is affected by the laser power, exposure time, and FPP. To illustrate the material's heating procedure while forming the hole, the COMSOL Multiphysics program was utilized to study the variations of thermal characteristics within the PC during machining, as well as various complexities of hole drilling. Several effective factors were examined during the laser drilling process. The laser's power (2, 3, and 4 W), exposure time (0.1, 0.15, 0.2s), and different FPPs (−4, −2, and 0 mm) were applied in this research. These parameters were chosen according to the experimental test conditions of this research. The images were obtained from the cross-section region of the workpiece, as shown in Fig. 9. The temperature distribution of the material is shown after being subjected to a laser. The vaporized substance was displayed along the z-axis where the beam had penetrated the sample depth. The PC sheet vaporized at 500 °C. The dark red color area in the figure signifies the removed material when it reached a temperature greater than the vaporization point. The results further indicate the warm and cold sides close to the
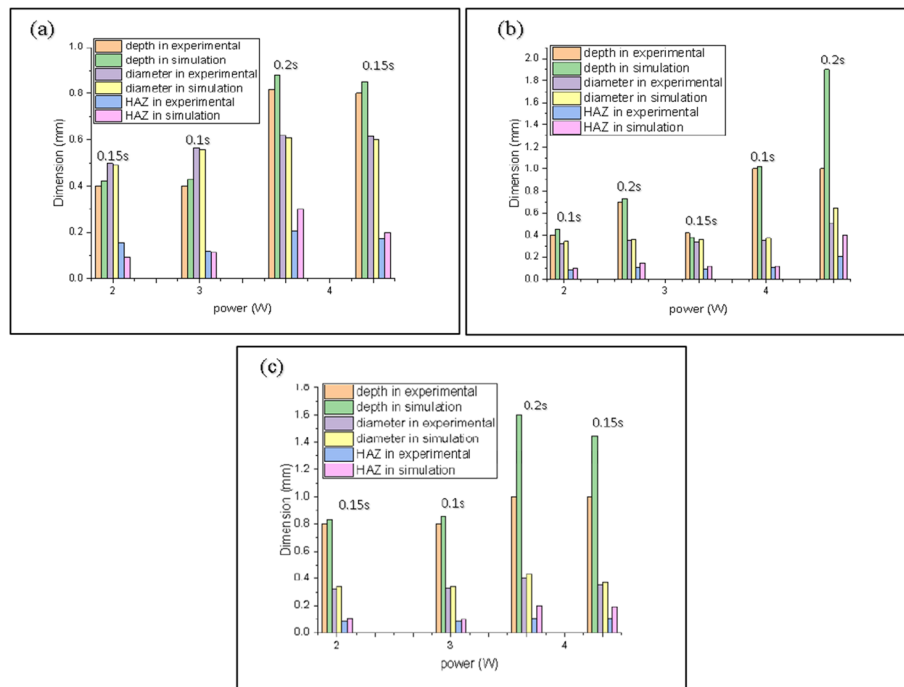

Fig. 10 A comparison graph of an experimental and theoretical micro-drilling hole (depth, diameter, and HAZ) for different power, time, and FPP: **a** −4 mm, **b** −2 mm, and **c** 0 mm

Table 7 Numerical equation of the heat transfer model

Boundary condition	Equation	Description	Equation parameters
Governing equation	$\rho C_p \frac{\partial T}{\partial t} = K\nabla^2 T + Q$	The partial differential eq. of heat conduction through the material	ρ: the specimen's density (kg cm^{-3}) Cp: the specific heat (J kg^{-1} K^{-1}) k: The thermal conductivity (Wm^{-1}K^{-1}) Q: represents a distributed heat generation term T: represents the temperature field as a function of time and space (K)
Conduction heat flux	$hf = \frac{P}{\pi r_b^2}\, e^{\frac{-2r^2}{r_b^2}}$	The heat flux occurs on the sample's top surface	hf: laser heat flux (Wm^{-2}) P: laser power (W) r_b: radius of the laser spot at the workpiece's surface (μm) r:the radial distances from the center of the laser beam point
Convection heat flux	$Q_c = A_s h_c (T - T_{amb})$	The heat flux occurs at the sample's boundary	Q_c: convective heat flux (W/m^{-2}) h_c: coefficient of convective heat transfer (W/m^{-2} K^{-1}) T: specimen temperature (K) T_{amb}: ambient temperature (K)
Radiation heat flux	$Q_r = A_s \varepsilon \sigma \left(T^4 - T_{amb}^4\right)$		ε: the material emissivity $\boldsymbol{\sigma}$: Stefan–Boltzmann constant (Wm^{-2} K^4)

Table 8 Limitations of parameters and responses

Name	P	t	FPP	Hole depth	Hole diameter	HAZ
Unit	W	s	mm	mm	μm	μm
Goal	In the range				Minimize	
Lower limit	2	0.1	−2	0.98	320	80
Upper limit	4	0.2	0	1	618	206

removed material. The warm edge represents HAZ and is shown as gradient temperature distribution colors. Similar outcomes were obtained from the experimental results, as shown in Fig. 10.

To illustrate, the numerical equation of the heat transfer model in this work is shown in Table 7 [33, 36].

Numerical optimization

The numerical optimization technique was used to generate high-quality solutions for both constrained and unconstrained optimization problems because of its global search capabilities. Optimization uses probabilistic principles to minimize or maximize the objective function rather than deterministic ones, overcoming the constraints of traditional approaches [37, 38]. After attempting to acquire relatively similar results between the practical and theoretical tests, hole drilling optimization
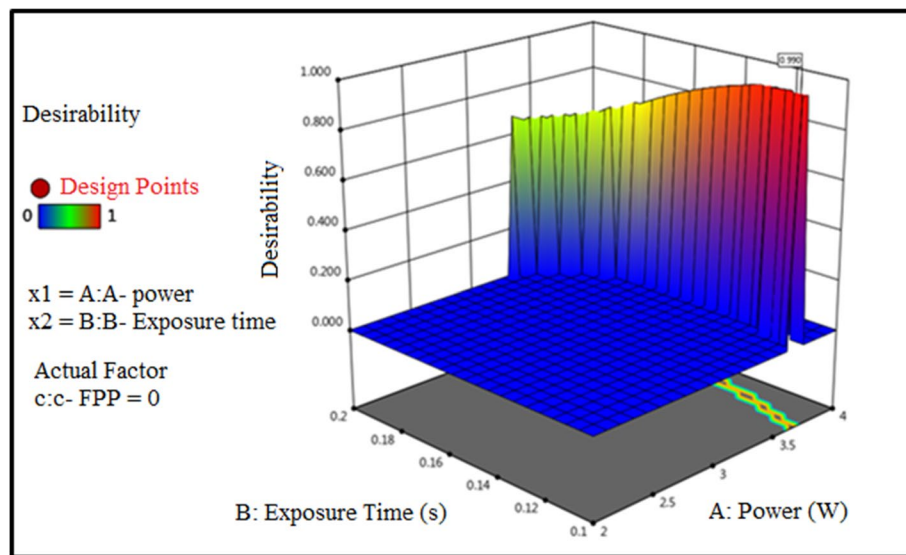
Fig. 11 3D surface of predicted optimum hole results
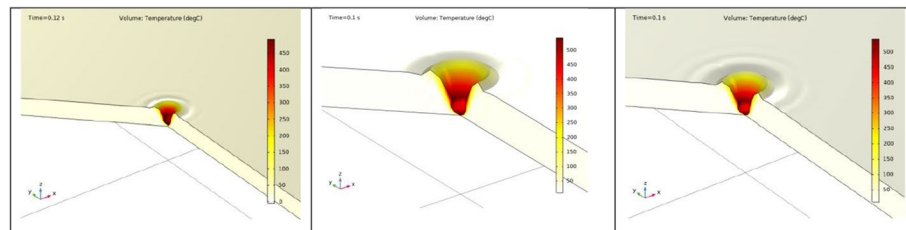

Fig. 12 Prediction results suggested by Design–Expert via COMSOL with powers (3, 3.6, and 4W) and time (0.12, 0.1, and 0.1 s), respectively at 0 FPP, of PC
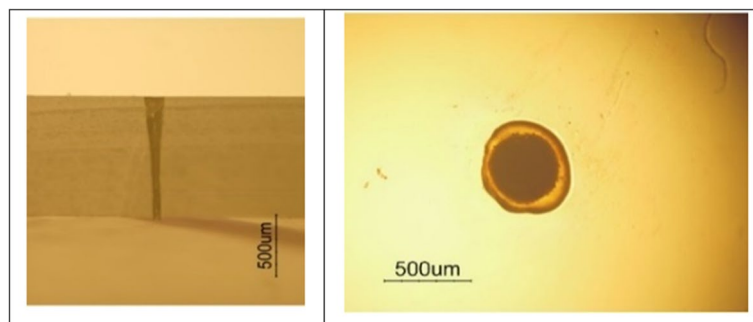

Fig. 13 Hole shape after optimization

was accomplished using Design–Expert, in which several parameters and response constraints were analyzed (as shown in Table 8). This process resulted in several outputs (as shown in Fig. 11), which were later used in another piece of software (COMSOL); some results are depicted in Fig. 12. COMSOL was used to determine which output fitted the identical status or the ideal hole (full hole and suitable diameter

with a small HAZ). After acquiring the best output from the simulation (which was the best output of Design–Expert), we changed to a real practical device (CO_2 drilling device). Figure 13 presents the ideal hole (1-mm depth, 350-μm entry diameter, and 90-μm HAZ) with parameters 3.6 W power, 0.1 s time, and 0 FPP.

Conclusions

In this research, a 1-mm thickness polycarbonate sample was selected. The laser beam employed was on continuous mode. The input characteristics of the BBD included laser beam power, exposure time, and the laser's FPP. The parameters (hole depth, entry diameter, and HAZ) were considered as output responses. Based on the results, the following conclusions were reached:

- The hole diameter at the focus position was lower than the hole diameter at the defocus position due to a decrease in laser beam spot diameter.
- The lowest HAZ that occurred at the focus position was at 0.15 s and 2 W laser drilling, providing a 0.8-mm depth with minimized diameter based on BBD.
- The highest hole diameter was obtained at a distance of −4 from the PC sheet surface, with 4 W and at 0.15 s.
- The cross-section changed from a V- to a U-shape when the focal position was altered from focus to defocus, respectively. However, this change was at the expense of hole deformation and an increase in hole diameter.
- The ideal hole (full hole, with a diameter of 350 μm, and a small HAZ of 90 μm) was obtained at 3.6 W, 0.1 s, and 0 FPP.

  The similarity between the simulation results and the practical experiment under identical conditions was significantly close, indicating accurate modeling.

Abbreviations
PC	Polycarbonate
CO_2	Carbon dioxide
BBD	Box–Behnken design
P	Power
t	Exposure time
FPP	Focal plane position
HAZ	Heat-affected zone
CW	Continuous
D_f	Focal diameter

Availability of data and materials
The datasets generated during the current study are available from the corresponding author on reasonable request.

Declarations

Competing interests
The authors declare that they have no competing interests.

Abdulwahab *et al. Journal of Engineering and Applied Science*   (2022) 69:98

Page 15 of 16

Author details

¹Department of Laser and Optoelectronics Engineering, University of Technology, Baghdad, Iraq. ²Ministry of Science and Technology, Baghdad, Iraq.

References

1. Schulz W, Eppelt U, Poprawe R (2013) Review on laser drilling I. Fundamentals, modeling, and simulation. J Laser Appl 25:1–17
2. Ahn DG, Jung GW (2009) Influence of process parameters on drilling characteristics of Al 1050 sheet with thickness of 0.2 mm using pulsed Nd: YAG laser. Trans Nonferrous Met Soc China 19:57–63
3. Almeida IA (2006) Optimization of titanium cutting by factorial analysis of the pulsed Nd:YAG laser parameters. J Mater Process Technol 179:105–110
4. Dubey AK, Yadava V (2008) Experimental study of Nd:YAG laser beam machining-an overview. J Mater Process Technol 195:15–26
5. Dubey AK, Yadava V (2008) Laser beam machining-a review. Int J Mach Tools Manuf 48:609–628
6. Meijer J (2004) Laser beam machining (LBM), state of the art and new opportunities. J Mater Process Technol 149:2–17
7. Gautam GD, Pandey AK (2018) Pulsed Nd:YAG laser beam drilling: a review. Opt Laser Technol 100:183–215
8. Stratakis E, Ranella A, Farsari M, Fotakis C (2009) Laser-based micro/nanoengineering for biological applications. Prog Quantum Electron 33:127–163
9. Singh H, Kwan SL, Tam D, Mamalis N, Maclean K (2015) Fracture and dislocation of a glass intraocular lens optic as a complication of neodymium:YAG laser posterior capsulotomy: case report and literature review. J Cataract Refract Surg 41:2323–2328
10. Urbaniak-Domagala W (2019) Electrical properties of polyesters. In: Alam MK (ed) Electrical and electronic properties of materials. Intech Open, London, pp 137–144
11. Mao J, Chen K, Chen S (1997) Microstructure and mechanical properties of Yb-Y-TZP. Microstructure and mechanical properties. Journal of Inorganic materials. 12:687–692
12. Umar Y (2014) Polymer basics: classroom activities manipulating paper clips to introduce the structures and properties of polymers. J Chem Educ 91:1667–1670
13. Al-Omairi LM (2010) Crystallization, mechanical, rheological and degradation behavior of polytrimethylene terephthalate, polybutylene terephthalate and polycarbonate blend. Ph.D. Thesis. Royal Melbourne Institute of Technology, Melbourne
14. Hanon MM (2012) Experimental and theoretical investigation of the drilling of alumina ceramic using Nd:YAG pulsed laser. Opt Laser Technol 44:913–922
15. Sabah FA (2012) Study the effect of many parameters on the speed of drilling materials by laser beam. Eng Technol J 30:1987–1999
16. Jabbar MS (2014) Influence of power density and exposure time on laser drilling hole. Eng Technol J 32:2313–2321
17. Hubeatir KA, Al-Kafaji MM, Omran HJ (2018) Deep engraving process of PMMA using CO_2 laser complemented by Taguchi method. Materials Science and Engineering 454:1–11
18. Chen X, Hu Z (2017) An effective method for fabricating microchannels on the polycarbonate (PC) substrate with CO_2 laser. Int J Adv Manuf Technol 92:1365–1370
19. Ghoreishi M (2006) Statistical analysis of repeatability in laser percussion drilling. Int J Adv Manuf Technol 29:70–78
20. Masmiati N, Philip PK (2007) Investigations on laser percussion drilling of some thermoplastic polymers. J Mater Process Technol 185:198–203
21. Patel MR, Chaudhary APS, Soni ADK, Student PG, Tech M (2015) A review on laser engraving process for different materials. Int J Res Dev 2:1–4
22. Khayoon MA, Hubeatir KA (2021) Laser transmission welding is a promising joining technology technique - a recent review. Journal of Physics: Conference Series (JPCS) 1973:1–17
23. Imran HJ, Hubeatir KA (2021) CO_2 laser micro-engraving of PMMA complemented by Taguchi and ANOVA methods. Journal of Physics: Conference Series 1795:1–14
24. Jiang SX, Yuan G, Huang J, Peng Q, Liu Y (2016) The effect of laser engraving on aluminum foil-laminated denim fabric. Text Res J 86:919–932
25. Caiazzo F, Curcio F, Daurelio G (2005) Laser cutting of different polymeric plastics (PE, PP and PC) by a CO_2 laser beam. J Mater Process Technol 159:279–275
26. Tanaka K (2017) Effects of the molecular weight of polycarbonate on the mechanical properties of carbon fiber reinforced polycarbonate. WIT Trans Eng Sci 116:327–335
27. Davim JP (2008) Some experimental studies on CO_2 laser cutting quality of polymeric materials. J Mater Process Technol 198:99–104
28. Meunier T, Weck A (2013) Plane stress local failure criterion for polycarbonate containing laser drilled microvoids. Polymer 54:1530–1537
29. Cormont JJM (1985) Differences between amorphous and crystalline plastics with respect to thermoforming. Adv Polym Technol 5:209–218
30. Liu Y, Huxtable ST (2014) Nonlocal thermal transport across embedded few-layer graphene sheets. Journal of Physics: Condensed Matter 26:1–6

31. Moradi M (2021) Simulation, statistical modeling, and optimization of CO_2 laser cutting process of polycarbonate sheets. Optik 225:1–25
32. Moradi M, Mehrabi O (2017) Enhancement of low power CO_2 laser cutting process for injection molded polycarbonate. Opt Laser Technol 96:208–218
33. Vasiga D, Channankaiah (2015) A review of carbon dioxide laser on polymers. Int J Eng Technol 4:874–877
34. Uno K, Kato M, Akitsu T, Jitsuno T (2017) Polycarbonate resin drilling by longitudinally excited CO_2 laser. 10091:1–6
35. Mushtaq RT, Wang Y (2020) State-of-the-art and trends in CO_2 laser cutting of polymeric materials-a review. 13:1–23
36. Abass AK (2010) Calculating the focusing effect of laser beam on the penetrating & cutting speed. 28:612–620
37. Mishra YK, Mishra S, Suryavanshi A (2022) Inclined laser drilling in glass fiber reinforced plastic using Nd: YAG laser. 44(2):66
38. Singh S, Yaragatti N (2022) Drilling parameter optimization of cenosphere/HDPE syntactic foam using CO_2 laser. J Manuf Process 80(September 2021):28–42

Publisher's Note

Springer Nature remains neutral with regard to jurisdictional claims in published maps and institutional affiliations.